Interaction and deformation of viscoelastic particles: Nonadhesive particles

Phil Attard
Ian Wark Research Institute, University of South Australia, Mawson Lakes, South Australia, 5095, Australia
(Received 20 November 2000; published 24 May 2001)

A viscoelastic theory is formulated for the deformation of particles that interact with finite-ranged surface forces. The theory generalizes the static approach based upon classic continuum elasticity theory to account for time-dependent effects, and goes beyond contact theories such as Hertz and that given by Johnson, Kendall, and Roberts by including realistic surface interactions. Common devices used to measure load and deformation are modeled and the theory takes into account the driving velocity of the apparatus and the relaxation time of the material. Nonadhesive particles are modeled by an electric double layer repulsion. Triangular, step, and sinusoidal trajectories are analyzed in a unified treatment of loading and unloading. The load-deformation and the load-contact area curves are shown to be velocity dependent and hysteretic.

DOI: 10.1103/PhysRevE.63.061604 PACS number(s): 83.60.Bc, 68.35.−p, 83.50.−v, 68.37.Ps

I. INTRODUCTION

The interactions of macroscopic bodies, microscopic particles, and macromolecules are mediated by their surface forces, and much attention has focussed upon measuring these forces directly and upon developing quantitative theories for them. The two generic forces that are well established, the van der Waals attraction and the electric double layer repulsion, have a range of up to 100 nm or so. Depending upon the elasticity of the bodies, their mutual interaction can be strong enough to deform them, particularly under an applied load or when pulled apart. Despite this the various theoretical treatments of particulate interactions generally assume rigid, undeformed bodies. Similarly, direct force measurements usually neglect the effects of deformation in their interpretation. This assumption can introduce serious errors, such as an underestimate of the magnitude of the force, or an inference of the wrong separation in a measurement.

The elastic deformation of bodies has been studied in engineering and mechanics, where it has obvious practical importance. The most common approaches combine the classical equations of elasticity theory with the assumption that the bodies only interact when in contact. The oldest such theory is due to Hertz, who gave the deformation of two nonadhesive particles under load. The two most common theories for adhesive particles are due to Johnson, Kendall, and Roberts, [1] (JKR) and to Derjaguin, Muller, and Toporov [2] (DMT). All of these theories are contact theories, which means that they ignore the finite range of the surface forces. Taking into account the influence of realistic surface force gives rise to highly nonlinear equations for the consequent elastic deformation. Nevertheless these have been solved by a number of authors and it has been shown that finite range effects can be important, particularly in the precontact regime and in the vicinity of the edge of the contact region [3–14]. Surface forces are also known to determine the shape and deformation of a crack or fracture tip and to influence strongly its propagation.

This paper also deals with noncontact forces, since it analyzes deformable particles that interact with a double layer repulsion. It goes beyond the earlier *elastic* studies by treating *viscoelastic* effects. There is reason to believe that very compliant materials cannot be purely elastic, but that viscoelastic effects must occur when they are deformed. There is a wealth of experimental data on adhesive soft bodies that show hysteretic behavior that depends upon the details of the loading-unloading cycle [15–29]. The present study is motivated by earlier computations [9] that showed a correlation between hysteresis and deformability. More recent works [13,14], which traced this hysteresis to velocity dependent effects, was limited by the artificial dissipation introduced into the elasticity model and by the lack of determinism in the time scale. The present work formulates the general equations for the deformation of viscoelastic particles and uses a well-defined model for the material viscoelastic response. A unified treatment of loading and unloading is given and indeed the algorithm can be used for an arbitrary trajectory. The behavior of particles that interact with an exponential repulsion is analyzed, this being the simplest model of the electric double layer interaction. The next paper in the series will treat adhesive particles.

There have been a number of earlier studies of particle deformation and crack propagation that have attempted to incorporate viscoelastic effects, both experimental [30,31] and theoretical [32–43]. All of these have been contact theories that have not taken into account the range of the interactions between the particles. In addition many of the studies have been limited by the approximate way that viscoelastic effects have been incorporated into the theory. A peculiarity of these contact theories is the strong distinction that is drawn between loading and unloading, (or bonding and nonbonding, or crack healing and growth), as a number of authors attest [35,40–42]; those that give actual results restrict them *only* to one case or the other. Although Graham [36] and Ting [37] claimed to have solved the nonmonotonic nonadhesive contact problem *in principle*, their procedures do not appear to have been applied *in practice*. As mentioned above, the noncontact algorithm given here is applicable to an arbitrary trajectory and a number of results for nonmonotonic loads are given.

In fracture mechanics it is common to introduce a velocity-dependent adhesion energy into the JKR contact theory, and such an *ad hoc* quantity can be empirically fitted to measured data [30]. Barthel and Roux [43] inserted this

quantity in the JKR and DMT equations and solved the consequent differential equation to model certain experimental data that showed a velocity-dependent adhesion. Falsafi *et al.* [31] replaced Young's modulus in the equilibrium (static) JKR result with a time dependent creep compliance function. As pointed out by Hui *et al.* [41], this is likely a poor approximation because in general the latter cannot be removed from the temporal convolution integral over the history of the particle (see below).

A number of studies are based on the work of Ting [35] and of Schapery [38,39]. Greenwood and Johnson [40] followed Schapery [38] in simplifying the time convolution integral by replacing the creep compliance function by a constant. They also used Baranblatt's approximate crack shape to study crack opening (particle unloading). Schapery [39] later introduced a power law creep compliance function that gives liquidlike behavior at long times. This was used by Hui *et al.* [41] in a JKR contact theory for the loading phase of adhesive solids. Lin *et al.* [42] extended this study to unloading, (crack propagation). Finally, and of more direct relevance to this work concerned with nonadhesive, repulsive interactions, there have been a number of prior studies of viscoelastic Hertzian contact [32–34,36,37].

II. MODEL AND ANALYSIS

A. Elasticity

Linear elasticity theory gives the local deformation of the two solids due to their mutual interaction. The local separation between the surfaces may be written [9,13]

$$h(r)=h_0(r)-u(r). \tag{1}$$

Here $h_0(r)=h_0+r^2/2R$ is the surface separation of the undeformed solids at a distance r from the axis. For two spheres with radii R_1 and R_2 the effective radius is $R^{-1}\equiv R_1^{-1}+R_2^{-1}$. For a sphere interacting with a planar substrate this is the actual radius. More generally, R may be given in terms of the principal radii of curvature of the solids [44]. The total elastic deformation is given by [9,45]

$$u(r)=\frac{-2}{\pi E}\int d\mathbf{s}\frac{p(h(s))}{|\mathbf{r}-\mathbf{s}|}=\frac{-2}{E}\int_0^\infty ds\, s k(r,s) p(h(s)), \tag{2}$$

where the elasticity parameter is given in terms of Young's modulus and Poisson's ratio of the bodies, $2/E\equiv(1-\nu_1^2)/E_1+(1-\nu_2^2)/E_2$, and where the kernel is expressible in terms of the complete elliptic integral of the first kind [9,45]. Here $p(h)$ is the pressure between two infinite planes at a separation h. The form appropriate for electric double layer interactions is given below.

B. Viscoelasticity

In viscoelasticity theory the effective Young's modulus is time dependent and its reciprocal is sometimes called the creep compliance function, $C(t)=1/E(t)$. Simple viscoelastic materials are characterized by short-time and long-time behavior, $C(t)\to 1/E_0$, $t\to 0$, and $C(t)\to 1/E_\infty$, $t\to\infty$. Due to relaxation or creep, viscoelastic materials are initially stiff and soften over time, $E_0>E_\infty$. The simplest type of viscoelastic material is characterized by the two elastic limits and a characteristic relaxation time τ,

$$C(t)=\frac{1}{E(t)}=\frac{1}{E_\infty}+\frac{E_\infty-E_0}{E_0E_\infty}e^{-t/\tau}. \tag{3}$$

Materials of this sort are analyzed in detail here. It should be pointed out that the algorithm can be modified to encompass materials with multiple relaxation times or with qualitatively different viscoelastic behavior, such as the liquidlike materials studied by Schapery [39] and by Hui *et al.* [41], $C(t)=C_0+C_1t^m$, $0<m<1$, which corresponds to $E_\infty=0$.

Viscoelastic deformation involves a time integral over the previous history of the material. The generalization of the elastic deformation equation given above to viscoelastic materials is

$$\begin{aligned} u(r,t)-u(r,t_0)&=\int_{t_0}^t dt'\frac{-2}{\pi E(t-t')}\int d\mathbf{s}\frac{\dot p(h(s,t'))}{|\mathbf{r}-\mathbf{s}|}\\ &=\int_{t_0}^t dt'\frac{-2}{E(t-t')}\int_0^\infty ds\, s k(r,s)\dot p(h(s,t')), \end{aligned} \tag{4}$$

where $\dot p(h(s,t))=p'(h(s,t))\dot h(s,t)$ is the time rate of change of the pressure. The particles are assumed stationary up to time t_0, $\dot h(r,t)=0$, $t<t_0$, and, if interacting or in contact, have at that time fixed deformation $u(r,t_0)=u_\infty(r,t_0)$, corresponding to static elastic equilibrium. It may be verified that this viscoelastic expression reduces to the static elastic result when $E(t)=\text{const}$. This expression is essentially equivalent to that used by earlier authors [34,37,41] in the context of contact theories of viscoelastic interactions. Here it is used for realistic finite ranged surface forces. The expression is justified by the so-called correspondence principle, in which the material property (Young's modulus) becomes time dependent, but the boundary conditions are unchanged (i.e., the kernel is that of the elastic half-space approximation of continuum elasticity).

Because the local separation depends upon the deformation, the above is a nonlinear integral equation for the latter that could, in principle, be solved by iteration. However the time-convolution integral complicates the matter and suggests a Laplace transform may be in order. An alternative is to cast the equations in the form of a differential equation. Using the creep compliance function given above, Eq. (3), differentiating with respect to time yields

$$\begin{aligned} \dot u(r,t)=&\frac{2}{\pi\tau}\int_{t_0}^t dt'\frac{E_\infty-E_0}{E_\infty E_0}e^{-(t-t')/\tau}\int d\mathbf{s}\frac{\dot p(h(s,t'))}{|\mathbf{r}-\mathbf{s}|}\\ &-\frac{2}{\pi E_0}\int d\mathbf{s}\frac{\dot p(h(s,t))}{|\mathbf{r}-\mathbf{s}|} \end{aligned}$$

$$= \frac{-1}{\tau}\left[\frac{2}{\pi E_\infty}\int_{t_0}^{t} dt' \int d\mathbf{s}\frac{\dot{p}(h(s,t'))}{|\mathbf{r}-\mathbf{s}|} + u(r,t)-u(r,t_0)\right] - \frac{2}{\pi E_0}\int d\mathbf{s}\frac{\dot{p}(h(s,t))}{|\mathbf{r}-\mathbf{s}|}$$

$$= \frac{-1}{\tau}[u(r,t)-u_\infty(r,t)+u_\infty(r,t_0)-u(r,t_0)] - \frac{2}{\pi E_0}\int d\mathbf{s}\frac{\dot{p}(h(s,t))}{|\mathbf{r}-\mathbf{s}|}. \quad (5)$$

Here u_∞ is the static deformation that would occur in the long-time limit if the pressure profile were fixed at its current value,

$$u_\infty(r,t) = \frac{-2}{\pi E_\infty}\int d\mathbf{s}\frac{p(h(s,t))}{|\mathbf{r}-\mathbf{s}|}. \quad (6)$$

As mentioned above, if the trajectory starts from the fully relaxed state, which is normally the case if $\dot{p}(t)=0$, $t<t_0$, then $u_\infty(r,t_0)-u(r,t_0)=0$. However this term is here retained explicitly to account for the possibility of a sudden impulse applied at $t=t_0$. The rate of change of the pressure is

$$\dot{p}(h(r,t)) = p'(h(r,t))[\dot{h}_0(t)-\dot{u}(r,t)]. \quad (7)$$

Hence if the current deformation is known, which means that $p'(h(r,t))$ is fixed, then Eq. (5) represents a *linear* integral equation for the rate of change of deformation. It can be solved by iteration using *precisely* the same algorithm that has been developed for the static elastic problem [9,13]. It is then a simple matter of time stepping to solve the differential equation for a specified trajectory $h_0(t)$, $u(r,t+\Delta_t) = u(r,t)+\Delta_t\dot{u}(r,t)$. Perversely, the viscoelastic problem actually turns out to be less demanding computationally than the corresponding elastic case.

C. Multiple relaxation times

The formalism and algorithm is readily extended to materials with multiple relaxation times. Suppose that the creep compliance function is of the form

$$C(t) = \sum_{i=0}^{n} c_i e^{-t/\tau_i}, \quad (8)$$

with, for example, $c_i = E_i^{-1} - E_{i+1}^{-1}$. Taking $E_n = E_\infty$, $E_{n+1} = \infty$, and $\tau_n = \infty$, this reduces to the simpler form given above in the case that $n=1$. Usually one would have $E_0 > E_1 > \cdots > E_n$, and $\tau_0 < \tau_1 < \cdots < \tau_{n-1}$, and if $\tau_i \ll t \ll \tau_{i+1}$, then $C(t) \approx 1/E_{i+1}$. The total deformation is

$$u(r,t)-u(r,t_0) = \sum_{i=0}^{n} u_i(r,t), \quad (9)$$

where the partial deformations represent the contribution from each mode and are defined by

$$u_i(r,t) = \frac{-2c_i}{\pi}\int_{t_0}^{t} dt'\, e^{-(t-t')/\tau_i}\int d\mathbf{s}\frac{\dot{p}(h(s,t'))}{|\mathbf{r}-\mathbf{s}|}. \quad (10)$$

In view of the fact that $\tau_n=\infty$, for $i=n$ this reduces to

$$u_n(r,t) = \frac{-2}{\pi E_\infty}\int d\mathbf{s}\frac{p(h(s,t))-p(h(s,t_0))}{|\mathbf{r}-\mathbf{s}|} = u_\infty(r,t)-u_\infty(r,t_0). \quad (11)$$

As above, differentiation with respect to time yields

$$\dot{u}_i(r,t) = -u_i(r,t)/\tau_i - \frac{2c_i}{\pi}\int d\mathbf{s}\frac{\dot{p}(h(s,t))}{|\mathbf{r}-\mathbf{s}|}, \quad (12)$$

where the rate of change of pressure depends upon the drive velocity and the total rate of change of deformation, as given above. Hence if the current partial deformations are known, this represents a set of coupled linear integral equations for the $\dot{u}_i(r,t)$. These may be obtained by iteration by essentially the same procedure as in the single relaxation time case. Note that because one needs only evaluate a single convolution integral per iteration, there is negligible increase in the computational time required in going from one to several relaxation times. Likewise, the memory required increases negligibly, since the deformations are linear in the number of grid points whereas the kernal is quadratic. The deformation trajectory again follows by simple time stepping, $u_i(s,t+\Delta_t) = u_i(s,t)+\Delta_t\dot{u}_i(s,t)$.

D. Load and pressure

In this paper the mutual pressure acting between the surfaces is taken to be a linear Poisson-Boltzmann form for the electric double layer repulsion, plus a short-range soft wall repulsion that is derived from a $1/r^{-12}$ intermolecular repulsion,

$$p(h) = Pe^{-\kappa h} + P_w(z_0/h)^9. \quad (13)$$

The second term is only effective at very small separations; in this work $z_0 = 0.5$ nm and $P_w = P$. A Debye length of $\kappa^{-1} = 1$ nm corresponds to 0.1 M monovalent binary aqueous electrolyte, and $P = 10^7$ N m^{-2} corresponds to a surface potential of about 85 mV, which is about the upper limit of what is typically encountered.

The total load is simply the integral of the surface force density,

$$F(t) = 2\pi\int_0^\infty p(h(r,t))r\,dr. \quad (14)$$

This applies for both the elastic and the viscoelastic case.

For the present repulsive pressure, as the bodies are driven towards each other the load becomes more positive and the deformation more negative. This is called loading. Conversely, unloading corresponds to an increasing (more

positive) deformation and decreasing load as the centers of the bodies are separated. To distinguish between the deformed and undeformed separations, $h_0(t)$ will be called the position, and $h(t)$ will be called the separation.

E. Slowly varying deformation approximation

The so-called slowly varying deformation approximation was introduced by Attard and Parker [9] to account for the elastic deformation in the weak deformation limit. It turned out to give analytic results and to be quite accurate for the precontact situation. Here an analogous approximation is developed for the viscoelastic problem. The approximation consists of replacing the deformation everywhere by its value on the central axis,

$$u(r,t)\approx u(0,t)\equiv u(t). \tag{15}$$

This is inaccurate away from the central axis, but since the pressure rapidly decays to zero in this region, the error introduced is negligible, at least for small deformations. In this approximation Eq. (5) becomes

$$\begin{aligned}\dot{u}(t)&=\frac{-1}{\tau}[u(t)-u_\infty(t)]+\frac{4P\kappa}{E_0}\int_0^\infty ds\,\exp\{-\kappa[h_0(t)\\&\quad+s^2/2R-u(t)]\}[\dot{h}_0(t)-\dot{u}(t)]\\&=\frac{-1}{\tau}[u(t)-u_\infty(t)]+\frac{4P\kappa}{E_0}\sqrt{\frac{\pi R}{2\kappa}}\exp\{-\kappa[h_0(t)\\&\quad-u(t)]\}[\dot{h}_0(t)-\dot{u}(t)],\end{aligned} \tag{16}$$

which may be solved for $\dot{u}(t)$,

$$\dot{u}(t)=\frac{f(t)\dot{h}_0(t)-[u(t)-u_\infty(t)]/\tau}{1+f(t)}, \tag{17}$$

where $f(t)\equiv\sqrt{8\pi\kappa RP^2/E_0^2}\exp\{-\kappa[h_0(t)-u(t)]\}$. In this equation

$$\begin{aligned}u_\infty(t)&=\frac{-2}{\pi E_\infty}2\pi\int_0^\infty ds\,P\exp\{-\kappa[h_0(t)+s^2/2R-u(t)]\}\\&=\frac{-E_0}{E_\infty\kappa}f(t).\end{aligned} \tag{18}$$

For a given trajectory $h_0(t)$, the deformation $u(t)$ is readily obtained from the equation for $\dot{u}(t)$ by simple time stepping; a calculator or spreadsheet suffices.

An analytic solution to this differential equation can be obtained at large separations when $f(t)$ can be neglected compared to unity in the denominator, and where $\kappa u(t)\ll 1$ and can be neglected in the exponent. For a linear trajectory, $h_0(t)=h_0+\dot{h}t$, taking $t_0=0$, the approximate differential equation becomes

$$\dot{u}(t)=\frac{-u(t)}{\tau}+\left[\frac{\kappa\dot{h}}{E_0}-\frac{1}{\tau E_\infty}\right]\sqrt{\frac{8\pi RP^2}{\kappa}}e^{-\kappa h_0}e^{-\kappa\dot{h}t}. \tag{19}$$

The solution that vanishes at $t=0$ is

$$u(t)=A[e^{-\kappa\dot{h}t}-e^{-t/\tau}], \tag{20}$$

where

$$A=\frac{\kappa\dot{h}\tau E_0^{-1}-E_\infty^{-1}}{1-\kappa\dot{h}\tau}\sqrt{\frac{8\pi RP^2}{\kappa}}e^{-\kappa h_0}. \tag{21}$$

Since $\dot{h}<0$, one sees that the deformation is always negative, which corresponds to flattening. The parameter $\kappa\dot{h}\tau$ controls which of the two values of the elasticity dominate. For materials with short relaxation times, or long-ranged interactions, or for slow driving velocities, this reduces to the static elastic result with $E=E_\infty$. In the opposite limit one obtains the static elastic result corresponding to $E=E_0$.

A formal series solution can be given to the above when the denominator is retained, but with $\kappa u(t)$ neglected in the exponent. However this is not particularly useful and it is a little inconsistent to retain higher powers of $f(t)$ while neglecting powers of $u(t)$, since the two functions are of the same order.

In the slowly varying deformation approximation the force is given by [9]

$$F(t)=2\pi R\kappa^{-1}P\exp\{-\kappa[h_0(t)-u(t)]\}. \tag{22}$$

This result turns out to be the same as the Derjaguin approximation, except that the planar interaction free energy per unit area is calculated at the actual separation $h(t)$, (as given by the approximation), rather than at the nominal separation $h_0(t)$.

The slowly varying deformation approximation can also be used to obtain the response to a harmonic perturbation, which enables a spectroscopic analysis of the viscoelastic interaction. A driving function $h_0(t)=h_0+\eta\sin\omega t$ to linear order produces a response in the central deformation $u(t)=u(t_0)+\nu\sin(\omega t+\phi)$. Linearization of the differential equation with respect to η and ν and equating the coefficients of the trigonometric functions yields

$$\tan(\theta+\phi)=\frac{-E_0}{E_\infty\omega\tau} \tag{23}$$

and

$$\nu=\eta\frac{c}{1+c}\frac{\cos\theta}{\cos(\theta+\phi)}, \tag{24}$$

where

$$\tan\theta=-(1+cE_0/E_\infty)/\omega\tau(1+c),$$

and

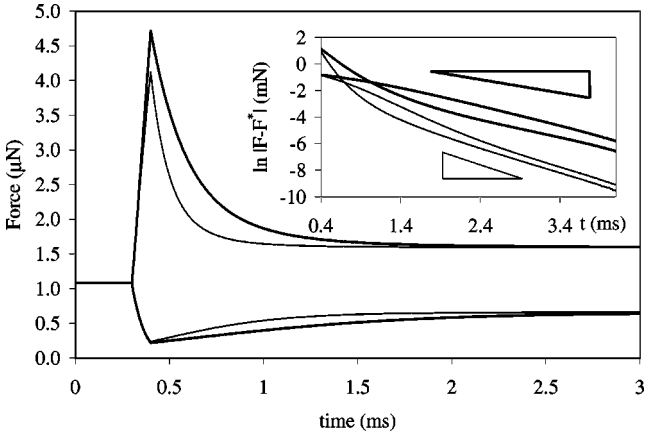

FIG. 1. Load relaxation following a sudden step in position. Following equilibration at $h_0=-5$ nm, over 0.1 ms a 2 nm step inward has been made to $h_0=-7$ nm (upper curves) or outward to $h_0=-3$ nm (lower curves). The plain and bold curves are for $\tau=1$ and 2 ms, respectively. The other parameters are $P=10^7$ N m^{-2}, $\kappa^{-1}=1$ nm, $E_0=10^{10}$ N m^{-2}, $E_\infty=10^9$ N m^{-2}, and $R=10$ μm. The inset shows the force on a log scale, with the final force being $F^*=1.59$ and 0.66 μm, for loading and unloading, respectively.

$$c=\sqrt{8\pi\kappa RP^2/E_0^2}\exp\{-\kappa[h_0-u(t_0)]\}.$$

The corresponding force is also harmonic, $F(t)=F(t_0)[1+a\sin(\omega t+\chi)]$, and using Eq. (22) one has

$$\tan\chi=\frac{-\nu\sin\phi}{\eta-\nu\cos\phi} \tag{25}$$

and

$$a=\kappa\sqrt{\eta^2+\nu^2-2\eta\nu\cos\phi}. \tag{26}$$

In the low frequency limit $\omega\to 0$, it is straightforward to show that $\phi\to 0$, $\chi\to 0$, $\nu\to-\kappa\eta u(t_0)/[1-\kappa u(t_0)]$, and $a\to\kappa\eta/[1-\kappa u(t_0)]$, where the central deformation in the slowly varying deformation approximation is the solution of $u(t_0)=-E_0c/E_\infty\kappa$.

III. RESULTS

Figure 1 shows the resultant force when two particles in contact and equilibrated at $h_0=-5$ nm are suddenly moved ± 2 nm. The change in position is almost a step change, since its duration (0.1 ms) is small compared to the relaxation time of the material. The initially large repulsion immediately following the step is characteristic of a stiff material, $E_0=10^{10}$ N m^{-2}. Over time the repulsion decreases as the material relaxes to accommodate the new configuration; on long time scales the particle appears softer, $E_\infty=10^9$ N m^{-2}. The behavior of two materials with different relaxation times are compared. It may be seen that τ may be obtained from the slope of the force difference on a log plot (inset). At $h_0=-5$ nm it is 0.50τ, and at $h_0=1.5$ nm it is 0.66τ (not shown). The material with the longer relaxation time shows a higher peak force due to the fact that there is a smaller contribution from E_∞ during the finite time of the step. There is an asymmetry evident between loading and unloading. It requires a greater increase in load to move the particles together a given amount than to separate them.

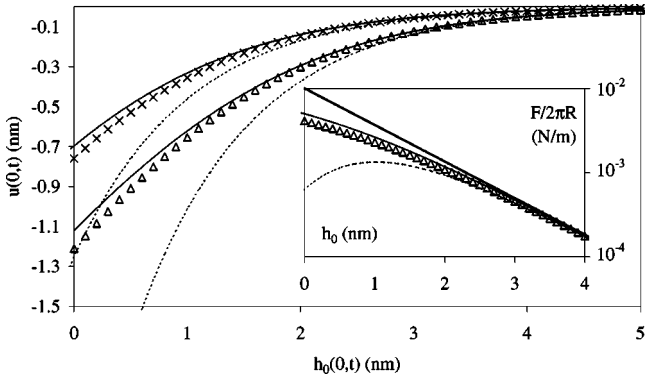

FIG. 2. Test of the slowly varying deformation approximation. The relaxation time is $\tau=1$ ms, all other relevant parameters as in Fig. 1. A constant driving velocity of $\dot{h}_0=5$ (upper) and of 1 μm s^{-1} (lower) is used. The symbols represent the exact calculation, the solid curves are the full differential equation, Eq. (17), and the dashed curves are the analytic approximation Eq. (20). The inset shows the corresponding forces normalized by the radius for $\dot{h}_0=1$ μm s^{-1}, with the bold curve representing the infinitely rigid case (no deformation).

Figure 2 shows the precontact deformation as the particles are uniformly driven together. The deformation is negative, which corresponds to flattening of the particles under their mutual repulsion. At a given position h_0, the deformation is greater at the slower driving speed because the soft component of the elasticity has more time to take effect. Conversely and consequently, the force is greater at the faster driving speed because the surface separation of the effectively stiffer material is smaller at a given position (not shown).

The slowly varying deformation approximation is quite good and it accurately accounts for the viscoelastic behavior prior to contact. The numerical solution of the differential equation, Eq. (17), may be described as quantitatively accurate. The analytic approximation, Eq. (20), works well at large separations but overestimates the deformation closer to contact when $\kappa u(t)$ is no longer negligible.

The actual load at a given position is compared with that for rigid particles in the inset of Fig. 2. It can be seen that the requisite load is reduced because the surface separation between deformed particles at a given position is greater than that between undeformed particles. This effect is quite clear in the elastic Derjaguin approximation, Eq. (22). It may be seen from the inset that this approximation is quite accurate for the two slowly varying deformation expressions.

Force spectroscopy was carried out on the particles at a mean position of $h_0=2$ nm, which corresponds to a mean load of 61.0 nN and a mean deformation of -0.46 nm. A sinusoidal change in position of amplitude 0.1 nm was made and the response in force monitored using the exact viscoelastic response, Eq. (5). Figure 3 gives the relative amplitude and the tangent of the phase angle. The curves are relatively smooth and featureless. The amplitude of the response

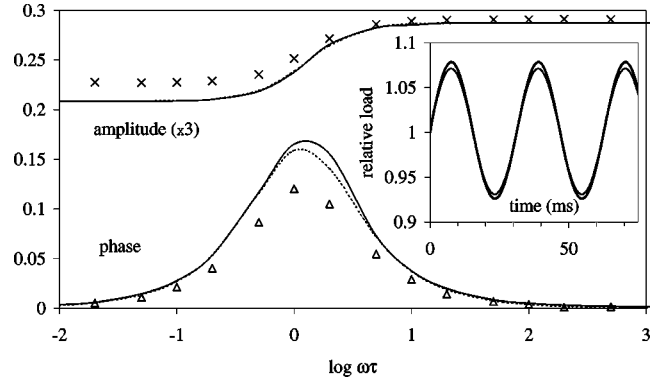

FIG. 3. Spectroscopic response in force to an oscillatory drive of amplitude $\eta=0.1$ nm applied about $h_0=2$ nm. The symbols are the exact calculation, and the curves are the slowly varying deformation approximation, the full curve being the complete result, Eq. (17), and the almost coincident dashed curve being the analytic approximation to it, Eq. (25). Here $\tau=1$ ms, the logarithm is base 10, and all other relevant parameters as in Fig. 1. The inset shows the exact (bold) and approximate (plain) force for a driving frequency of $\omega=200$ rad s^{-1}.

is constant at low and high frequencies, with the latter having the larger amplitude, as one might expect from the greater stiffness on small time scales. The transition between the two regimes occurs at $\omega=0.78\tau^{-1}$ (cf., discussion of Fig. 1). At this frequency the phase angle is a maximum at 7°, and it decays to zero at the two frequency extremes.

Figure 3 also tests the numerical slowly varying deformation approximation Eq. (17), and the analytic approximation Eq. (25). The latter two are nearly coincident, which shows the value of the analytic approximation. The slowly varying deformation approximation tends to overestimate the phase factor and to underestimate the amplitude at low frequencies, but overall describes the harmonic response very well. It is tedious but straightforward to show that in this approximation the peak in the phase lag occurs at a frequency ω_0 given by $(\omega_0\tau)^2=(1+cE_0/E_\infty)/(1+c)$. For $h_0=2$ nm this gives $\omega_0^{-1}=0.85\tau$, in reasonable agreement with the exact calculation.

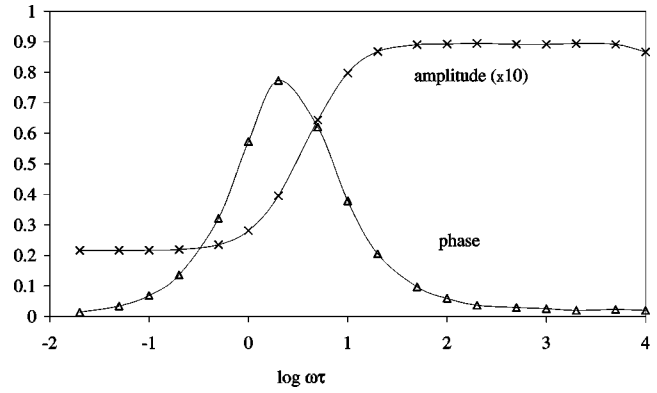

FIG. 4. Exact response to a driven oscillation under a high load, $[F_\infty(h_0)=1.08\ \mu$N, $h_0=-5$ nm and $\eta=1$ nm, the logarithm is base 10, all other parameters as in the preceding figure]. The line simply connects the measured data points.

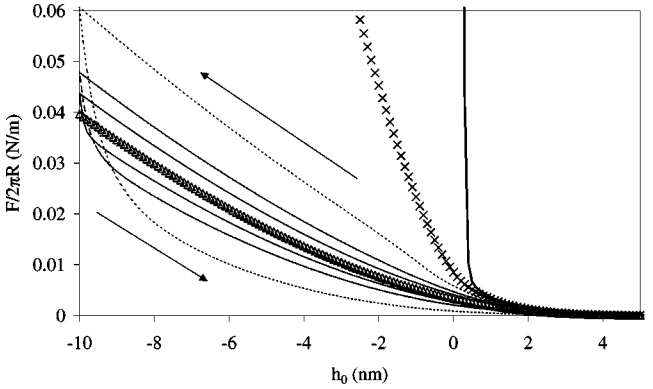

FIG. 5. Force hysteresis loops for a triangular drive. The parameters are as in Fig. 1, with $\tau=1$ ms, and with drive velocities of $\dot{h}_0=\pm1$, ±2, and ±5 μm s^{-1}, from inside to outside, respectively. The bold curve is the rigid, undeformable particle result, and the triangles and crosses are the static, equilibrium result for $E=10^9$ and 10^{10} N m^{-2}, respectively.

Figure 4 carries out the force spectroscopy at $h_0=-5$ nm. The relatively high load of 1.08 μN used here is sufficient to cause noticeable surface flattening. The slowly varying deformation approximation is not designed to cope with such large and variable deformations, and it is inappropriate to compare it with the exact calculations in this regime. The behavior in contact is qualitatively similar to that shown in Fig. 3 prior to contact, with some quantitative differences. The peak in the phase is more pronounced, with the phase angle now being 38°, and it has shifted to $\omega=2/\tau$, (cf., the inset to Fig. 1). Also at this frequency the step in amplitude corresponds to about a factor of 4 increase in this case, compared to a factor of 1.3 in Fig. 3.

Perhaps the most common type of deformation measurement is concerned with particle loading and unloading using a triangular drive velocity. Such a measurement is modeled in Fig. 5 for several drive speeds. Negative values of the position would correspond to interpenetration of the undeformed surfaces, as evinced by the almost vertical force between the rigid particles of the figure as $h_0\to0^+$. For deformable surfaces such negative values are allowed and, since the deformation is negative, they correspond to positive separations, $h(r,t)=h_0(r,t)-u(r,t)$. The force is increasingly repulsive in this regime. What is also noticeable is the hysteresis between the loading and the unloading branches, and the fact that this increases with drive speed. On the loading branch, the force-position curve for the viscoelastic particles lies between the equilibrium elastic results for E_∞ and E_0. Slow driving speeds show a more gradually increasing repulsion and lie closer to the long-term elastic value, as one might expect. As the speed increases the loading curves move towards the equilibrium result for the instantaneous elastic modulus, which has a more sharply increasing repulsion. On the unloading branch, there is initially a rapid decrease in the force immediately following the turning point. This behavior originates in the nature of the change in the surface shape, as will be discussed shortly. Much of the unloading branch lies beneath the static curve corresponding to E_∞, and for slow enough driving speed one can well imagine

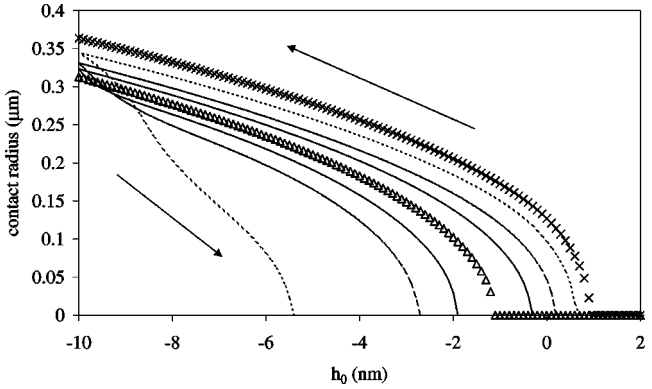

FIG. 6. Contact radius hysteresis loops for the same cases as the preceding figure. Contact was defined as a local surface separation of less than 1 nm.

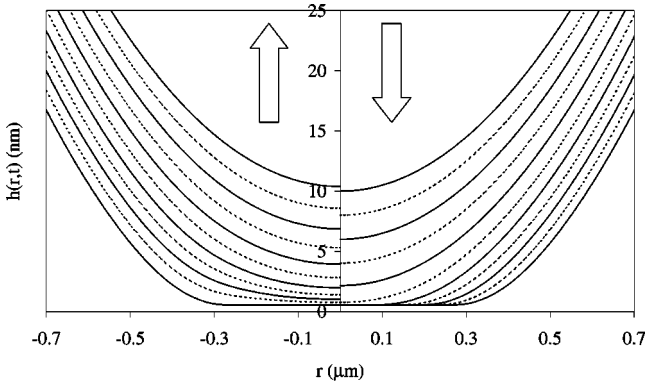

FIG. 7. Surface profiles for the $|\dot{h}_0| = 5\ \mu\mathrm{m\,s^{-1}}$ case of Fig. 6. A snapshot of the local separation is plotted as a function of the lateral radius every 0.4 ms, or every 2 nm from $h_0 = 10$ to $h_0 = -10$ nm and back. The right hand panel is for loading, and the left hand panel is for unloading. The loading profile at $h_0 = 10$ nm is essentially undeformed.

that the two branches will coalesce on it. The fact that the force upon unloading is less than that on loading at a given position gives the appearance that the surfaces come in to contact (i.e., measurably interact) on approach at a greater position than they come out of contact upon retraction. The reason for this will also be discussed shortly.

Figure 6 shows the contact radius for the triangular drive just discussed. The surfaces were defined to be in contact wherever the local separation was less than 1 nm, which is the decay length of the double layer repulsion used here. For any finite ranged surface force the definition of contact is arbitrary, but any reasonable definition gives qualitatively similar behavior to that shown in Fig. 6. In general the contact area increases with increasing applied load. As for the force, the hysteresis between loading and unloading increases with driving velocity and the static instantaneous elastic result provides an upper bound for the loading branch that is approached as the driving velocity is increased.

At first sight it might appear counterintuitive that the particles that are driven faster, and that are therefore effectively stiffer, exhibit a greater contact area on approach than the more slowly driven particles. The explanation becomes clear upon examining the loading region where the contact first becomes nonzero. For the fastest driving velocity this occurs just beyond $h_0 = 1$ nm, which indicates little flattening has occurred. Conversely, contact does not occur until about $h_0 = -0.5$ nm for the slowest driving velocity, due to substantial surface flattening. In other words, one should not confuse deformation with contact area for particles that interact with finite surface forces.

The contact radius hysteresis is similar to the force hysteresis in that it is due to the rapid decrease immediately following the turnaround. This behavior is particularly marked for the fastest driving velocity. A picture of what is occurring may be gleaned from Fig. 7. The asymmetry between the loading and unloading surface shapes is due to the finite time over which the measurement is performed. It is clear that on loading the surfaces become relatively flattened, and their shape particularly at the center is largely determined by the geometry and the position rather than by the elastic parameters. Immediately after the turnaround, the flattened regions separate as a whole rather than peeling from the edge, which is what they would do in the elastic case. This is the reason that the contact radius and the force drop so rapidly on the initial part of the unloading branch. Over the time of unloading the flattened regions relax to their more naturally curved shape. Even though the final unloading profile at $h_0 = 10$ nm is beyond the range of the surface force, at the high velocity of the figure full relaxation has not yet occurred, and one can see that the surfaces still retain a memory of their contact. (The duration of the unloading branch was 2 ms, which is twice the relaxation time, $\tau = 1$ ms.) This remnant flattening means that for a given position the surfaces are at a greater separation on unloading than on loading, and hence the force and the contact area go rapidly to zero upon unloading, as shown in Figs. 5 and 6.

Finally, Fig. 8 shows the unloading force for several maximum applied loads. The unloading branches initially differ from each other, as they must as a consequence of the hysteresis. But after sufficient time all the unloading curves coalesce on a single envelope. This behavior is very similar to that of adhesive particles previously explored [13,14]. At large separations where the force is weak, the loading and

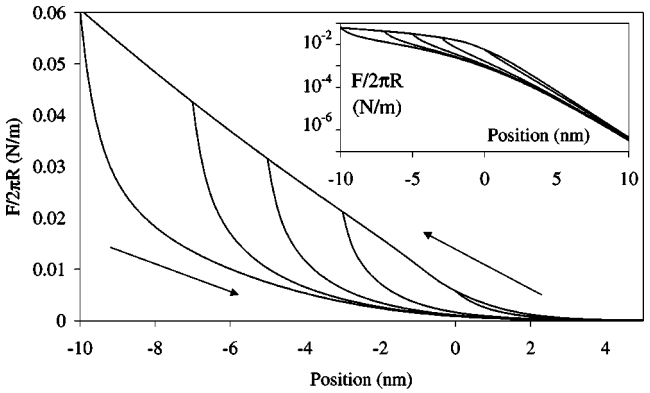

FIG. 8. Force loops for different penetrations. The parameters are as in Fig. 6, with a drive velocity of $|\dot{h}_0| = 5\ \mu\mathrm{m\,s^{-1}}$, and turning points of $h_0 = 0, -3, -5, -7$, and -10 nm.

unloading forces are exponentially repulsive, as is evident by the linear tail in the logarithmic inset.

IV. CONCLUSION

This paper has been concerned with the viscoelastic deformation of particles and surfaces during their interaction. A general formulation of the problem for finite-ranged surface forces was given, and a numerical algorithm was presented for materials with one or more relaxation times. The algorithm is applicable to both loading and unloading, and indeed to an arbitrary trajectory. Results were presented for a repulsive double layer interaction for step, triangular, and sinusoidal drives. An analytic approximation applicable to slowly varying deformations was developed and shown to be accurate in the precontact regime.

In general at a given position the repulsion upon loading was less than that between rigid particles, and it lay between that of elastic particles corresponding to the short and long-time limits of the creep compliance function. Force spectroscopy revealed a peak in the phase lag and a step in the amplitude, which is characteristic of materials with a single relaxation time. Hysteresis was observed between the loading and unloading branches, and it increased with driving velocity and the relaxation time of the materials, with the unloading force and contact radius being less than the loading at a given position. This behavior originated in the differences in the contact region dynamics due to the viscoelastic nature of the materials. On loading the surfaces fold into contact from the edge, whereas during unloading they pull apart as a whole rather than peel apart from the edge, retaining their flattened shape for a short time after contact.

The present theory for viscoelastic deformation and interactions is very general and the algorithm is robust and computationally simple. In the next paper in the series it will be applied to adhesive particles. In future work it is hoped to present analytic results for viscoelastic Hertz and JKR contact theories, and to analyze quantitatively experimental data using the full theory with realistic finite-ranged surface forces.

ACKNOWLEDGMENT

The support of the Australian Research Council through the Special Research Center for Particle and Material Interfaces at the Ian Wark Research Institute is gratefully acknowledged.

[1] K. L. Johnson, K. Kendall, and A. D. Roberts, Proc. R. Soc. London, Ser. A **324**, 301 (1971).
[2] B. V. Derjaguin, V. M. Muller, and Yu. Toporov, J. Colloid Interface Sci. **53**, 314 (1975).
[3] V. M. Muller, V. S. Yushchenko, and B. V. Derjaguin, J. Colloid Interface Sci. **77**, 91 (1980).
[4] V. M. Muller, V. S. Yushchenko, and B. V. Derjaguin, J. Colloid Interface Sci. **92**, 92 (1983).
[5] B. D. Hughes and L. R. White, Q. J. Mech. Appl. Math. **32**, 445 (1979).
[6] B. D. Hughes and L. R. White, J. Chem. Soc., Faraday Trans. 1 **76**, 963 (1980).
[7] J. B. Pethica and A. P. Sutton, J. Vac. Sci. Technol. A **6**, 2490 (1988).
[8] J. R. Smith, G. Bozzolo, A. Banerjea, and J. Ferrante, Phys. Rev. Lett. **63**, 1269 (1989).
[9] P. Attard and J. L. Parker, Phys. Rev. A **46**, 7959 (1992); Phys. Rev. E **50**, 5145(E) (1994).
[10] J. L. Parker and P. Attard, J. Phys. Chem. **96**, 10 398 (1992).
[11] J. A. Greenwood, Proc. R. Soc. London, Ser. A **453**, 1277 (1997).
[12] J. Q. Feng, Colloids Surf., A **172**, 175 (2000).
[13] P. Attard, J. Phys. Chem. B **104**, 10635 (2000).
[14] P. Attard, Phys. Rev. E **63**, 1601 (2001).
[15] M. D. Pashley and J. B. Pethica, J. Vac. Sci. Technol. A **3**, 757 (1985).
[16] R. G. Horn, J. N. Israelachvili, and F. Pribac, J. Colloid Interface Sci. **115**, 480 (1987).
[17] Y. L. Chen, C. A. Helm, and J. N. Israelachvili, J. Phys. Chem. **95**, 10 736 (1991).
[18] N. A. Burnham and R. J. Colton, J. Vac. Sci. Technol. A **7**, 2906 (1989).
[19] N. A. Burnham, D. D. Dominguez, R. L. Mowery, and R. J. Colton, Phys. Rev. Lett. **64**, 1931 (1990).
[20] A. L. Weisenhorn, P. Maivald, H.-J. Butt, and P. K. Hansma, Phys. Rev. B **45**, 11226 (1992).
[21] M. K. Chaudhury and M. J. Owen, Langmuir **97**, 5722 (1993).
[22] H. R. Brown, Macromolecules **26**, 1666 (1993).
[23] C. Creton, H. R. Brown, and K. Shull, Macromolecules **27**, 3174 (1994).
[24] M. Deruelle, L. Leger, and M. Tirrell, Macromolecules **28**, 7419 (1995).
[25] M. Tirrell, Langmuir **12**, 4548 (1996).
[26] M. Deruelle, H. Hervet, G. Jandeau, and L. Leger, J. Adhes. Sci. Technol. **12**, 225 (1998).
[27] K. J. Wahl, S. V. Stepnowski, and W. N. Unertl, Tribol. Lett. **5**, 103 (1998).
[28] F. J. Schmidtt, T. Ederth, P. Weidenhammer, P. Claesson, and H. J. Jacobasch, J. Adhes. Sci. Technol. **13**, 79 (1999).
[29] M. Rundolf, M. Karlsson, L. Wagberg, E. Poptoshev, M. Rutland, and P. Claesson, J. Colloid Interface Sci. **230**, 441 (2000).
[30] D. Maugis and M. Barquins, J. Phys. D **11**, 1989 (1978).
[31] A. Falsafi, P. Deprez, F. S. Bates, and M. Tirrell, J. Rheol. **41**, 1349 (1997).
[32] S. C. Hunter, J. Mech. Phys. Solids **8**, 219 (1960).
[33] E. H. Lee and J. R. M. Radok, J. Appl. Mech. **27**, 438 (1960).
[34] W. H. Yang, J. Appl. Mech. **33**, 395 (1966).
[35] T. C. T. Ting, J. Appl. Mech. **33**, 845 (1966).
[36] G. A. Graham, Int. J. Eng. Sci. **5**, 495 (1967).
[37] T. C. T. Ting, J. Appl. Mech. **35**, 248 (1968).
[38] R. A. Schapery, Int. J. Fract. **11**, 369 (1975).
[39] R. A. Schapery, Int. J. Fract. **39**, 163 (1989).

[40] J. A. Greenwood and K. L. Johnson, Philos. Mag. A **43**, 697 (1981).
[41] C.-Y. Hui, J. M. Baney, and E. J. Kramer, Langmuir **14**, 6570 (1998).
[42] Y. Y. Lin, C.-Y. Hui, and J. M. Baney, J. Phys. D **32**, 2250 (1999).
[43] E. Barthel and S. Roux, Langmuir **16**, 8134 (2000).
[44] L. R. White, J. Colloid Interface Sci. **95**, 286 (1983).
[45] L. D. Landau and E. M. Lifshitz, *Theory of Elasticity*, 2nd ed. (Pergamon, London, 1970).